



Effect of the Series Resistance on the Current Response of a HgCdTe Avalanche Photodiode Under High-intensity Nanosecond Irradiation

Asta Katrine Storebø¹ · Trond Brudevoll¹ · Espen Selvig¹ · Runar Wattum Hansen¹ · Torgeir Lorentzen¹ · Randi Haakenaasen¹

Received: 14 December 2021 / Accepted: 20 April 2022 / Published online: 10 May 2022
© The Author(s) 2022

Abstract

We investigate the nonlinear signal current response of a $\text{Hg}_{0.72}\text{Cd}_{0.28}\text{Te}$ avalanche photodiode (APD) irradiated by high-intensity, finite-duration laser pulses. At high irradiation levels and/or high gains, carrier-induced perturbations in the junction electric field and avalanche gain strongly influence the temporal behavior of the APD current. The total series resistance will play a major role here, and four values of the series resistance were used for mapping out the APD response. When striving for maximum achievable bandwidth, the internal junction capacitance and the internal series resistance set the ultimate limits for an APD. A signal analysis of these high-intensity nonlinear gain effects should therefore begin with an intrinsic APD, and proceed with adding appropriate external series resistances. A simultaneous modeling of the entire external circuit is then required. To this end, we have combined full-band Monte Carlo (MC) transport simulation in the active multiplication zone with conventional circuit modeling outside. We demonstrate how overshoot/undershoot and rapid oscillations in the signal current evolve in time as a function of the chosen external series resistances at two different high-intensity irradiation levels. Oscillations are shown to persist slightly beyond the duration of the laser pulse when operating the diode within the junction transit time-limited regime. The periodicity of the oscillations is related to the junction transit time and remains only weakly dependent on irradiation levels and external resistance values until we enter the resistance–capacitance (RC)-limited case. Here, a change occurs where oscillations are smoothed out as external series resistances are increased further.

Keywords HgCdTe · photodiode · avalanche photodiode · APD · infrared detector

Introduction

Avalanche photodiodes (APDs) are widely used in optical communication systems and laser radar detectors (LADARs). APDs normally operate in a linear avalanche gain mode below the breakdown threshold voltage or, for amplifying very weak signals, briefly above the breakdown threshold in Geiger mode. In linear mode, the APD operates within the linear portion of the avalanche gain versus bias voltage curve. In Geiger mode, a nonlinear gain response is achieved either by introducing a high external series resistance in the combined signal/bias path or by employing a switchable network to bring the bias safely below the breakdown threshold again as the avalanche progresses.

Otherwise, given enough integration time, the gain would theoretically be infinite in Geiger mode because the avalanche is self-sustaining there.

In a laboratory environment, interpreting and separating different internal processes (for example, electron movement, hole movement) could be carried out by analyzing the shape of the signal current. However, this may often become difficult due to the influence of subsequent readout circuit elements. Here, ultrashort (ps or sub-ps) lasers are usually the preferred optical signal sources, quite necessary for avoiding additional optically induced broadening of the APD impulse response.^{1–3}

However, optical signal intensity levels and signal durations impinging on an operational APD are usually not of the above type. The signals will typically be of finite (ns) duration and come from lasers potentially able to induce a nonlinear current response due to gain saturation effects, even when the APD is biased far below the avalanche breakdown threshold in an intentionally normal linear mode.

✉ Asta Katrine Storebø
asta-katrine.storebo@FFI.no

¹ FFI (Norwegian Defence Research Establishment), P.O. Box 25, 2027 Kjeller, Norway

In an APD, carrier multiplication takes place in the depletion zone. A large depletion zone means a small junction capacitance because of the large separation between positive and negative space charges. This separation increases with rising reverse bias. Whereas conventional photodiodes can have junction capacitances in the low pF range, APDs can have much smaller junction capacitances, even below 0.1 pF. Consequently, stray capacitances may often dominate and severely modify or deteriorate the APD raw signal.^{1–3}

If the gain of the APD saturates and turns nonlinear due to high input signal levels, interesting additional effects may be caused by nearby circuit elements, as these have a direct feedback on the diode current. In the latter context, the series resistance of the APD circuit becomes especially important, often ranging from less than 100 Ω in intrinsic cases to tens of k Ω when enhanced by external series resistances in, e.g., Geiger mode operation.^{4,5} To minimize unwanted capacitive side effects of the series resistance, this resistance is often monolithically integrated with the APD in the form of a thin-film resistor.⁵

HgCdTe APDs have been regarded as future candidates both for state-of-the-art, high-resolution LADARs,^{6,7} and for high-bandwidth space communications,⁸ all of them with one-photon GHz capability. Conclusions from these investigations suggest that HgCdTe diodes have a fast enough response for such applications, provided that certain design criteria are met, regarding both readout circuitry and APD design, where for the latter, operation closer to the transit time limited regime and elimination of the slow diffusion-limited response of the APD absorption region are mandatory. As fast communication APDs today operate at 10 GHz bandwidth and with a gain of 10, additional one-photon capabilities⁸ require avalanche gains close to 100, which is substantially more demanding. Obviously, pushing far into the GHz range with such high gains may under certain circumstances invoke impact ionization and transit time behavior, closely related to that seen in the family of microwave pn junction diodes normally operating in this frequency region, such as impact ionization transit time (IMPATT) diodes.⁹ Biased at their breakdown threshold, these devices serve as oscillators where the pn junction voltage swings above breakdown in one half-period and below breakdown in the next.

The purpose of the present paper is to explore how known electronic pn junction transport effects from the above microwave device types interact under slightly different conditions, where a strong optical input sets off the voltage and current excursions, and where the junctions are biased far below their breakdown threshold, at approximately half the breakdown voltage. Furthermore, since our interest here mainly concerns device response to high-intensity optical signal inputs, we shall not discuss one-photon capabilities or excess noise issues of APDs, since this would be more

relevant for weak optical signals and low signal-to-noise ratios. Instead, we refer the reader to our previous work¹⁰ on that subject, which gave an excess noise factor $F = 1.2$, in close agreement with experimental values. With the Cd alloy fraction of the absorption layer graded from 0.33 near the outer surface down to 0.28 at the pn junction, a mid-infrared (MWIR) detection capability is added, hence the simulated device is cooled to 77 K.

The present study of high-intensity, optically induced current response in a MWIR APD biased in a linear avalanche gain mode clearly shows an interplay between junction capacitance, avalanche gain saturation,¹¹ junction transit time, and the APD series resistance. The simulations delineate the differences between signal current response at moderate intensity levels versus the response at high intensity levels where a strong coupling occurs. Establishing the optical signal intensity level and the natural time scales where this interplay is expected to appear should help predict the behavior of similar future HgCdTe APD designs when pushed to their ultimate limits.

Model and Methods

Device Layout

The APD under study is depicted in Fig. 1.

The APD has a $48 \mu\text{m} \times 48 \mu\text{m}$ surface area and a $6.2\text{-}\mu\text{m}$ -thick *p*-type doped absorption layer with a free carrier concentration of $p = 2 \times 10^{16} \text{ cm}^{-3}$ at 77 K. A $6\text{-}\mu\text{m}$ -thick and $21\text{-}\mu\text{m}$ -wide lightly *n*-doped region surrounds the center contact with a free carrier concentration of $n = 5 \times 10^{14} \text{ cm}^{-3}$. The width of the center contact n^+ layer is $13 \mu\text{m}$, having a free carrier concentration of

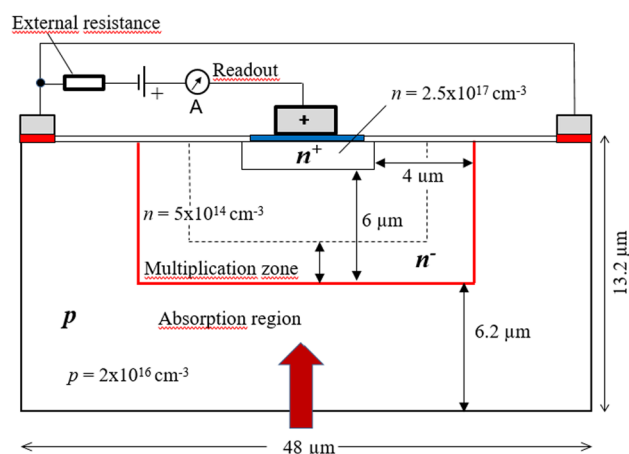


Fig. 1 Planar electron-initiated avalanche photodiode with bias voltage supply, external series resistance, and readout. Radiation enters the device through the lower surface (arrow).

$2.5 \times 10^{17} \text{ cm}^{-3}$. The lightly n -doped region reduces from $6 \mu\text{m}$ to $4 \mu\text{m}$ in the vertical corridors near the two side contacts, both of which have a width of $2 \mu\text{m}$. Finally, the interior Cd alloy fraction is $x = 0.28$, exponentially graded from $x = 0.33$ (i.e., cutoff starts at $4 \mu\text{m}$ wavelength) at the outer lower surface where the radiation enters the device. Alloy gradients in the p -type absorption layer arise naturally in liquid phase epitaxy-grown HgCdTe materials. The alloy gradient sets up an effective electric field, adding a small amount of drift to the photocarrier diffusion onto the pn multiplication zone, thus helping to speed up the response of the device.¹⁰

Primary, photogenerated electrons created in the absorption layer move by ambipolar diffusion aided by the alloy gradient towards the multiplication zone, where they impact ionize and generate new electron–hole pairs.

Electrons continue further upwards, and finally all of them are collected at the center contact. Holes, either primary, photogenerated holes or off-spring holes from the avalanche process, are collected by one of the two side contacts. Primary, photogenerated holes do not enter the multiplication zone at all.

Numerical Model Overview

We have developed a full-band Monte Carlo (MC) transport simulator¹² with finite difference and a finite element 2D/3D Poisson solver, which is used for initial-state, large-signal (i.e., bias) simulation of the APD.

Both the MC simulator and a conventional in-house developed lumped parameter circuit simulator work in parallel for the subsequent small-signal analysis during laser irradiation. This simulation therefore includes the external circuit shown schematically in Fig. 1, where the circuit simulator provides the time-dependent boundary conditions for the MC simulator, with the two simulators sharing the same time steps for updating the electric fields.

For simplicity, generation of primary, photogenerated electron–hole pairs inside the absorption layer occurs at regular time intervals following an absorption profile in the form $e^{-\alpha x}$ with absorption coefficients α extracted from Li et al.¹³ As long as practically all the photons are absorbed within $6 \mu\text{m}$, the choice of wavelength was found to play a minor role; here, the absorption condition is satisfied for wavelengths shorter than $3.5 \mu\text{m}$. After the absorption, subsequent transport and injection of primary photocarriers into the pn junction multiplication zone are handled by the MC simulator. The $6\text{-}\mu\text{m}$ -thick absorption layer acts both as an accumulator of the generated photocarriers and as a buffer, damping otherwise sudden increases in photocarrier injection into the pn junction multiplication zone, smearing the photocarrier arrivals out in time. In this way, generated photocarriers first accumulate, then migrate towards

the multiplication zone, while obeying the arrival statistics of carrier drift and diffusion. As no photons are directly absorbed inside the multiplication zone, the influence of variations in photon absorption statistics should be minor for the purpose of the present paper, where the main agenda is to study an APD pn junction overwhelmed by injected photoelectrons.

Outside the depletion zone, the small-signal MC simulation overlaps with the circuit simulator, exchanging information on the small-signal voltage drops inside the APD. Carriers exiting the multiplication zone are handed over to the lumped parameter solver on exit.

All contacts are treated as ideal, with zero resistance. However, being a part of the series resistance, the contact resistance adds directly. Therefore, a finite, ohmic contact resistance will have the same effect on the signal current as the increasing series resistances in the simulation examples below.

Holes practically do not induce impact ionizations in this material due to the large difference between the small Γ valley electron effective mass and the much larger heavy-hole effective mass. Electrons therefore gain energy more rapidly from the electric field, and thereby dominate the impact ionization process.

Band structures for the HgCdTe alloy were imported directly from an *ab initio* pseudopotential electronic structure code, ABINIT,¹⁴ after introducing band gap corrections appropriate for the particular alloy composition and temperature. The band gap at 77 K is 0.2 eV throughout the multiplication zone, where the Cd alloy fraction is 0.28. Impact ionization rates were described with a square-law Keldysh relationship,¹⁵ setting the prefactor to $8 \times 10^{10} \text{ s}^{-1}$ for electrons, and to zero for holes. Since our simulator works with energy-dependent impact ionization *probabilities*, and not field-dependent impact ionization *coefficients*, we keep track of the impact ionization history of each electron. Such history-dependent approaches include the all-important dead-space effect,¹⁶ which is a prerequisite for a realistic treatment of the APD and crucial for obtaining the experimentally observed excess noise factors less than 2. Another important element for the low excess noise in HgCdTe alloys is the huge, 1.2-eV separation between the Γ valley and the L valley band minima, which keeps most electrons inside the Γ valley, and thereby ensures a relatively uniform dynamic behavior of the hot electrons, translating into less randomness and noise.

Modeling Internal Charges, External Charges, Impact Ionization, RC-Limited Response, and Transit Time Limited Response in the Reverse-Biased APD

Internal carriers injected or generated via impact ionization form interacting ensembles of positive and negative charges,

which separate due to the bias electric field in the pn junction. As the charges separate, they induce an increasing small-signal perturbation of the junction bias potential, a perturbation which is manifested outside the junction and around the whole external circuit, driving the external current. Once internal charge carriers start to move inside the pn junction, external carriers also start to move via the displacement current mechanism in anticipation of the arriving internal carriers onto the external circuit.

The movement of internal charge carriers is determined by the total (bias + small-signal) internal electric field in the pn junction, whereas the external charge motion is determined by the generated voltage perturbations and the series resistance. Under constant bias, in the short-circuit limit, with the total (i.e., internal and external) series resistance tending to zero, the small-signal junction voltage must vanish. Then, the role of the external circuit loop would just be to allow some amount of charge ΔQ_{ext}^{pn} to flow externally from the *p*-side to the *n*-side in order to keep the small-signal junction voltage equal to zero throughout the entire internal charge movement. However, even with the small-signal junction voltage set to zero, the total junction electric field must be reduced locally, especially in the region between the separating electron and hole ensembles. The external current must compensate for this loss by seeking to enhance the junction electric field globally, thus keeping the total small-signal junction voltage unaltered. The net result will be a reduction in the total electric field in the central, intermediate region where impact ionization was successful, and an enhancement outside.

On increasing the series resistance, the compensating external current becomes restricted, and the charge transfer ΔQ_{ext}^{pn} becomes smaller. The junction electric field will now be reduced even more, but mostly in the central intermediate region with less reduction outside. We will also see a small, but finite, reduction in the junction voltage, due to the external current failing to immediately balance the perturbation of the junction potential caused by the moving internal carriers. Corresponding to the junction voltage drop, an equal voltage enhancement occurs over the series resistance, driving the external current through this resistance. Due to the partial junction voltage compensation effected by the external current however, the local electric field reduction in the central part of the junction becomes masked and cannot be directly estimated from the net drop in the junction voltage.

The effect of a local reduction in the electric field on the gain can be estimated by considering the exponential nature of the impact ionization process. For a gain in excess of 100, say 128 or 2^7 , an injected photoelectron must on the average lead to 7 new off-spring generations of carriers. Therefore, impact ionization is a very rare event, competing with other, more frequent, loss mechanisms. High gain values depend on impact ionization occurring at

regular intervals throughout the junction, adapting to the other scattering mechanisms and to the junction bias electric field profile. If a sudden local field reduction causes a single generation of electrons to miss their next expected impact ionization opportunity, the APD gain would immediately be cut in half. Furthermore, the local field reduction will occur in a region where impact ionization was successful earlier, and therefore these field perturbations will systematically seek and pinch off productive impact ionization chains.

Although some nonlinear gain/bias data for another material, GaN, were obtained in earlier Monte Carlo (MC) studies;¹¹ most work on APDs involving MC transport models do not deal with the high-intensity regime, and consider only linear gain effects. Herbert et al.¹⁷ simulated an InSb APD using both self-consistent electric fields and ns irradiation, but only at low intensities.

We shall begin our study with the transit time-limited case, as determined by the pn junction capacitance and increasing external resistances. In the transit time-limited case, the decay of the current response after a photonic impulse is determined by the combined transit time for avalanche-generated electron–hole pairs across the depletion zone.

In the resistance–capacitance (RC)-limited APD circuit on the other hand, the linear impulse response can be severely broadened by internal or external series resistances, differing significantly from the idealized short-circuit (RC = 0) situation often described in MC simulations. Such broadening of the impulse response occurs because these resistances restrict the free flow of charge carriers between the external diode terminals, and then the generated charge must instead be temporarily stored inside the APD, either as moving hot carriers or as thermalized carriers connecting with the junction capacitance. Here, we should bear in mind that the junction capacitance is a small-signal capacitance, providing the differential junction voltage change due to an incremental change in stored charge at the two ends of the multiplication zone. Further voltage changes across the junction are then caused by the hot carriers on the move inside the junction. Taking this view, the junction essentially resembles a capacitor with free, hot charge carriers moving inside.

Initially, the APD is treated as a single domain within the MC method. This establishes the extent of the pn junction and the bias field distribution. However, for a more economic treatment of a device this large, the small-signal analysis is carried out by partitioning the simulation into three separate domains, pn junction, APD areas outside the junction, and external circuit, where the latter domain will be trivial to handle due to the lumped parameter description. In this way, an adaptation of the methods used in each domain to the accuracy needed in that particular domain

becomes possible, with enhanced detail inside the pn junction and less detail outside.

The simulation flow is governed by a very general framework which can briefly be summarized as follows. First, subtracting the bias voltage from the junction voltage, a small-signal voltage relationship can be established between any two mesh points at opposite ends of the pn junction:

$$\frac{dv^{pn}}{dt} = \frac{dv_{int}^{pn}}{dt} + \frac{dv_{ext}^{pn}}{dt} \quad (1)$$

where v^{pn} is the total small-signal voltage over the pn junction, with v_{int}^{pn} describing the voltage contribution from all types of charges and processes internal to the junction, and v_{ext}^{pn} is the junction voltage contribution due to thermalized charge movement (i.e., current) through the resistive areas of the APD and the external circuit loop. Since there is just a finite resistance outside the pn junction, we must also have $v_{ext}^{pn} = v_{ext}^{pn}(v^{pn})$. Put another way, the total junction voltage change v^{pn} determines the boundary conditions to be obeyed at the interface between the pn junction and the rest of the APD, including the external circuit. The overrunning MC simulation in the resistive, quasi-neutral APD domain outside the pn junction then treats v^{pn} as a background voltage, while also taking care of the transport of the optically generated carriers, which are electrically neutral electron–hole pairs. It is the total voltage v^{pn} that sets up the external current which flows through the resistive areas of the APD outside the pn junction, and further into the external circuit loop. The simulation of the APD areas outside the junction is performed in response to the boundary condition v^{pn} , which enables us in turn to obtain the voltage over the external circuit, and thereby the current going through this loop. Monitoring the external current through a common time step Δt for all domains, we obtain the external charge transfer $\Delta Q_{ext}^{pn}(v^{pn})$ during this time step. Furthermore, from the bias simulation we inherit the necessary initial conditions for the different domains. Then, we may set up a small-signal self-consistent algorithm from one time step to the next for the junction voltage boundary condition v^{pn} :

$$v^{pn}(t + \Delta t) = v^{pn}(t) + \Delta v_{int}^{pn} + \Delta v_{ext}^{pn}(\Delta Q_{ext}^{pn}) \quad (2)$$

where the coupling term $\Delta v_{ext}^{pn}(\Delta Q_{ext}^{pn})$ denotes the contribution from the incremental charge transfer ΔQ_{ext}^{pn} from one APD contact through the external circuit into the other contact. As this charge returns into the APD via the other contact, it is distributed around the pn junction by the MC simulator. This coupling term connects to the lumped parameter description of the external circuit, and therefore also infers the RC-like behavior of the setup. It can further be seen that the internal junction charge movement voltage contribution Δv_{int}^{pn} constitutes the actual driving force for the central quantity v^{pn} and the other electronic small signals.

Simple, analytic RC diode models have been described earlier and discussed in great detail,¹ therefore, we shall not go any further on this subject here. We just note that the external current eventually equilibrates the diode back to its initial bias state. The photonic impulse essentially charges the pn junction capacitance by generating extra internal carriers. A large capacitance signifies a poor ability to discharge by rapidly pushing a current through a series resistance, prolonging the current pulse and thus the equilibration. A large capacitance also signifies that large amounts of charge can be stored on the capacitor in relation to the minimal voltage perturbation available to shuffle that charge around the external circuit.

Simulation Results and Discussion

We shall discuss results for two distinct laser intensity levels: first, a strong illumination of 7300 photons delivered in a 1-ns square laser pulse, and then an order of magnitude increase to 73,000 photons delivered within the same pulse length. These laser pulses are simple to implement theoretically, and have sufficient duration and intensity to allow any nonlinear avalanche gain response to freely evolve for some time under the incoming radiation. And, quite importantly, choosing a square pulse, we also avoid unwanted optical modulation of the APD electronic response, facilitating the interpretation of the simulation results. The irradiation corresponds to 0.94 fJ (0.94 μ W) pulse energy (power) for the lower intensity level and 9.4 fJ (9.4 μ W) pulse energy (power) for the higher intensity level, both taken at a wavelength of 1.55 μ m. Four values of external series resistances were considered (0 Ω , 500 Ω , 3 k Ω , and 32 k Ω), where 0 Ω is the intrinsic case without an added external resistance including only the series resistance of the diode at \sim 200 Ω .

A reverse bias of 6.8 V was used (see Fig. 2 for the bias potential distribution across the APD).

The potential distribution leads to a triangular electric field strength profile in the central part of the APD near $x = 25 \mu$ m, when taken as a function of the vertical position y across the pn junction. With a maximum reaching 30 kV/cm near the pn interface, it declines linearly to zero approximately 1.5 μ m before the end of the lightly doped n^- -region below the electron-collecting center contact. On both sides of the center contact, however, we observe that the junction depletion zone already reaches into the n^+ layer. The lightly n^- -doped portion of the pn junction, serving as the multiplication zone, provided an average linear multiplication gain of $M \sim 100$ at 6.8-V reverse bias. The junction capacitance is 0.07 pF at this bias, and the RC time constants of the APD circuit will therefore be 14.2 ps, 49.7 ps, 227.2 ps, and 2.27 ns for the different external resistances, respectively. Higher

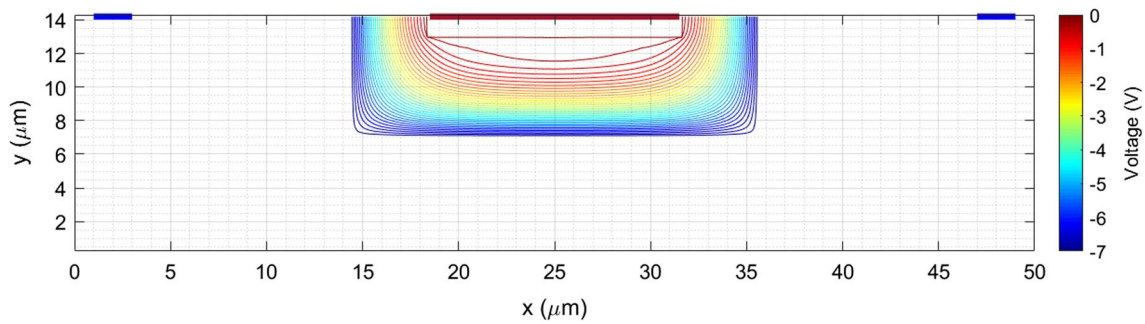


Fig. 2 The potential profile after bias simulation of the APD. Colorless areas indicate regions where the potential is nearly flat, keeping the value of the nearest equipotential line. Here, 1 μm at the bottom and 1 μm on both sidewalls are substrate and sidewall insulation, respectively.

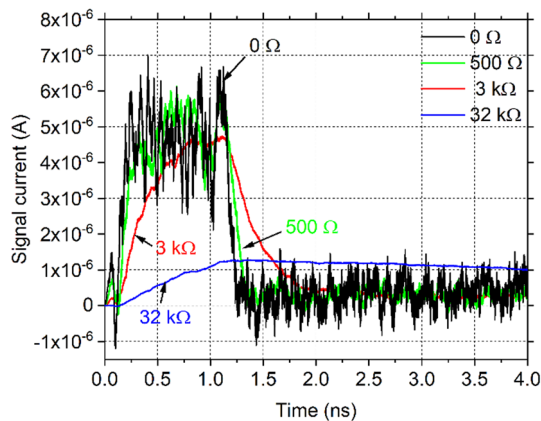


Fig. 3 Signal current (in amps) due to a square laser pulse of 7.3 kphotons in 1 ns with 6.8-V APD reverse bias voltage, showing how the signal current pulse shape changes with increasing external series resistance from the junction transit time-limited cases towards the two RC-limited cases at 3 k Ω and 32 k Ω , respectively.

reverse bias voltages would increase the gain and electric field, extending the multiplication zone slightly into the n^+ layer everywhere, with the electric field rapidly tending to zero inside the n^+ layer.

Figure 3 shows the signal current of the APD for an irradiation with 7300 photons per pulse. The response characterizing the two lowest external series resistances (0 Ω and 500 Ω) is clearly reflecting the noisy, rapid transit of hot charge carriers moving at high velocities across the pn junction. There is no particular difference between the intrinsic (i.e., 0 Ω) and the 500 Ω cases. On the other hand, increasing the external resistance to 3 k Ω with an estimated RC time constant of 227 ps, we see that the appearance of the signal current (red curve) has changed considerably. This change is due to the accumulation of avalanche-generated charge carriers inside the APD, as dictated by the increased external series resistance. Having traversed the pn junction, the accumulated charges are thermalized, and substantially increase the voltage

perturbation over the junction, and therefore the signal current is now mainly driven by them. Targeting the non-trivial trends in the signal current, we have not added a thermal noise source to the accumulated charges. Treating them as noiseless thus gives us a smoothed rendering of the signal current whenever these carriers dominate the signal current. Carriers having traversed the junction or carriers located outside the junction will affect the junction via their combined, finite electric potential, whereas their thermal noise properties must average to zero and will therefore be too weak to influence the junction physics in any decisive way.

Regarding the 32-k Ω external resistance, we observe that here the RC time constant has taken full control over the shape of the signal current, and transit time effects are no longer present, as we shall see when we investigate the detailed junction processes next.

In Figs. 4a, 5a and 6a, we show the signal currents for the 0 Ω , 500 Ω , and 3 k Ω external series resistances at the same, lower intensity level. In these figures, we also show the respective hot carrier populations underway inside the depletion zone. We observe a delay of about 203 ps from the end of the illumination pulse until a decay effect is manifested in the signal current.

The delay in the signal current derives from the transit of avalanche-generated carriers across the depletion zone, where separating the positive and negative charges generates an electric field opposite to that of the initial bias. This opposing electrical field leads to a drop in pn junction potential, but also to a corresponding voltage increase over the APD series resistance. The voltage drop over the pn junction quickly leads to less carrier generation, reducing the junction voltage drop. However, increasing separation between the generated hot electron and hole ensembles will tend to increase the junction voltage drop again, and, in the lower intensity cases, stabilizing it for a limited time after the pulse. During this time, which corresponds to the junction transit delay, we therefore observe a relatively steady series resistance voltage and a practically undiminished external

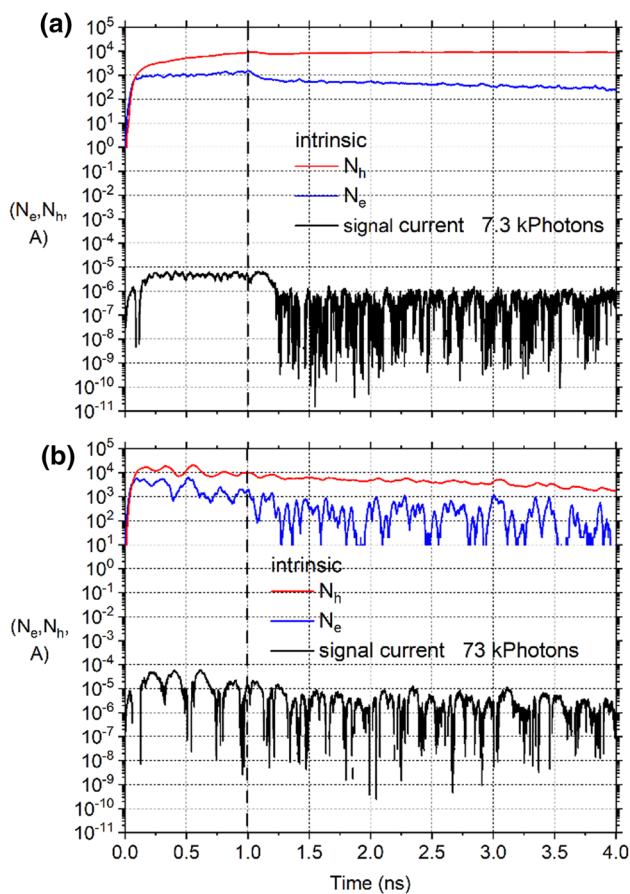


Fig. 4 Signal current (in amps) (lower curve) and hot carrier populations (upper curve N_h holes, middle curve N_e electrons) underway inside the pn depletion zone for an intrinsic avalanche photodiode without external resistance at (a) the lowest irradiation level of 7.3 kPhotons in 1 ns. (b) Increased laser intensity by an order of magnitude shows oscillations developing both during the laser pulse and going on for about 250 ps after the end of the laser pulse, after which the hole oscillations decay and the electron population is decimated and fluctuates around smaller values. In both parts of the figure, the dashed vertical line indicates the end of the laser pulse.

current, even though the number of hot electrons in the pn junction started their decline much earlier, becoming substantially reduced after just 50 ps, as shown in Figs. 4a, 5a and 6a.

Despite almost saturating the APD with photogenerated carriers, the gain causes little energy loss for the impact ionizing electrons, and still make them traverse the depletion zone much faster than holes. Both carrier types accumulate at opposite ends of the depletion zone where they thermalize and lose momentum. Electrons lose their ability to impact ionize further. For holes, the accumulation occurs at a much slower rate. This accumulation can be seen as a modulation¹¹ of the respective depletion zone widths. Accumulated, thermalized electrons and holes are therefore no longer counted as part of the hot carrier ensembles. Thus, the hot electron

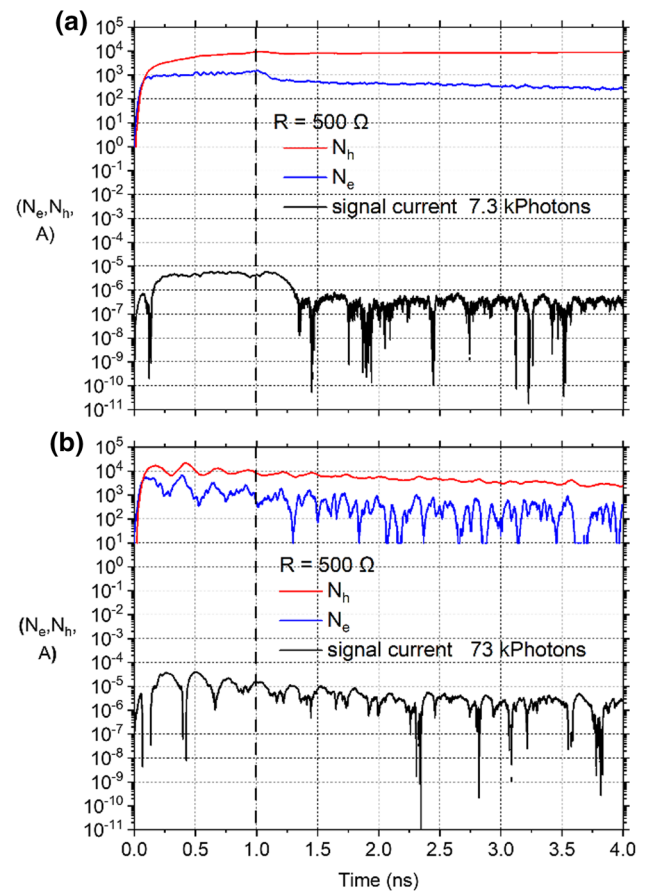


Fig. 5 Signal current (in amps) (lower curve) and hot carrier populations (upper curve N_h holes, middle curve N_e electrons) underway inside the pn depletion zone for an avalanche photodiode with external resistance of 500 Ω at (a) the lowest irradiation level of 7.3 kPhotons in 1 ns. (b) Increased laser intensity by an order of magnitude shows oscillations developing both during the laser pulse and beyond, after which the hole oscillations decay and the electron population is decimated and fluctuates around smaller values. In both parts of the figure, the dashed vertical line indicates the end of the laser pulse.

population on the move inside the depletion zone generally becomes smaller than the hot hole population as we present them here. The balance is taken up by a corresponding difference in the respective thermalized carrier populations.

As seen in Figs. 4a, 5a and 6a, within 50 ps after the laser pulse has ended, the number of hot junction electrons have started their decline. Separate simulations of single photoelectron diffusion times from the absorption layer onto the multiplication zone show a similar delay.¹⁰ After this delay, the supply of new photogenerated electrons from the absorption layer onto the multiplication zone has practically ceased. This electron diffusion time is largely consistent with the experimental results of Rothman et al.³ for a shortwave infrared APD, where the photoelectrons diffused across a 2- μm -thick graded absorption layer in just 20 ps. As expected, for the smaller-gap medium wave infrared

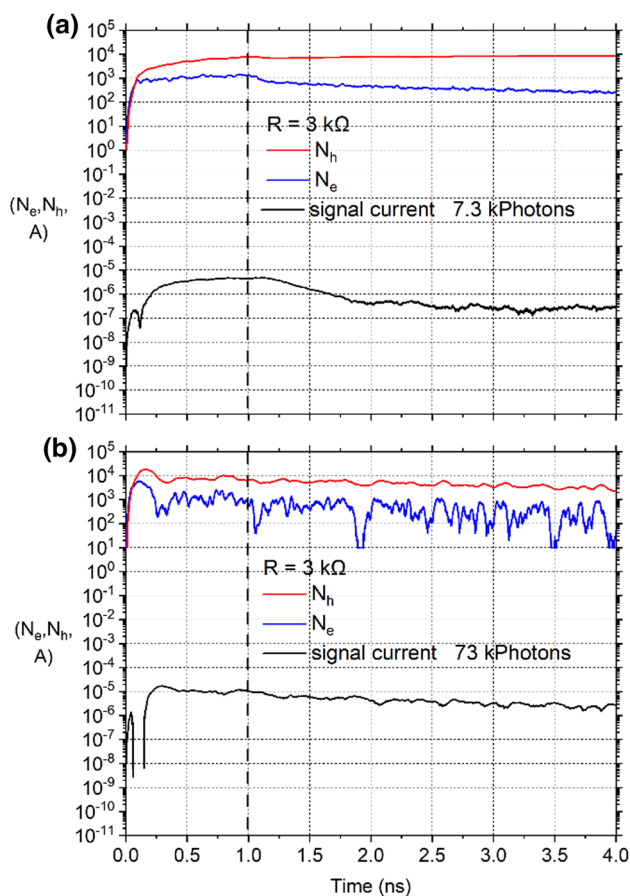


Fig. 6 Signal current (in amps) (lower curve) and hot carrier populations (upper curve N_h holes, middle curve N_e electrons) underway inside the pn depletion zone for an avalanche photodiode with external resistance of 3 k Ω at (a) the lowest irradiation level of 7.3 kPhotons in 1 ns; the shape of the laser pulse is still recognizable. (b) Increased laser intensity by an order of magnitude results in a single overshoot in the hot carrier populations early on and damped ripples (rather than oscillations) afterwards. The signal current is now relatively smooth, but information on the original laser pulse shape is lost. In both parts of the figure, the dashed vertical line indicates the end of the laser pulse.

material studied here, the photoelectrons are seen to diffuse even faster, covering a distance of 6 μm in just 50 ps, where we should allow for some differences in the actual alloy gradients between the two cases.

As a result of the different physics affecting the moving hot holes, a slowly increasing or decreasing hot hole population is observed, while the hot electron population decays. In Fig. 4a, the signal is relatively smooth and still follows the general shape of the laser pulse. However, a transient in the external current from 50 ps to 150 ps can be seen. The current quickly collapses after expelling some of the excess hot carriers generated earlier during the irradiation, and then reverts to a noisy behavior, caused by the number of hot holes still residing in the depletion zone, and the declining

number of after-pulsing electrons still producing some new electron–hole pairs for a few ns after the pulse. Judged by the current alone, it would seem that a steady state was reached during the laser pulse, but we see from the continuous accumulation of hot holes that this is not actually true. Being already close to a steady state after 1 ns, a reduction of the gain and an increase in the signal current should stabilize all variables within a somewhat longer laser pulse of 3–4 ns.

In Fig. 4b, the laser pulse intensity is raised 10-fold, to 73 kPhotons in 1 ns. Here, the APD becomes unable to follow the laser pulse, and in this case the actual shape of the optical pulse therefore becomes irrelevant. Hot carriers and an additional accumulation of thermalized carriers at both ends of the pn junction contribute to an overall enhanced signal current level, which does not show any collapse as the irradiation stops. Clearly, the avalanche severely saturates the device, and correlated oscillations in the hot carrier populations and the signal current evolve during the pulse and continue for a while after the irradiation has ceased. Due to the saturation effect on the junction electric field, the oscillation period is expanded to roughly 220 ps, with some timing jitter.

As the internal carrier ensembles become well-defined and separate, a small but steady voltage drop develops over the pn junction, and a correspondingly small voltage increase outside the pn junction drives the signal current through the resistive areas of the APD and into the external circuit. Note the “phase lag” in the oscillation peak between the electrons and holes; an increase in hot, impact-ionizing electrons slightly precedes a corresponding increase in generated holes. The minimum in the signal current roughly coincides with the maximum in internal carrier populations. After a period of strong carrier multiplication, the large electron and hole ensembles have not separated far enough to decisively screen out the bias potential from any large region of the pn junction, so no appreciable weakening of the junction voltage occurs. However, as the charges eventually separate further, the potential over the pn junction finally becomes smaller, and a corresponding voltage enhancement rapidly shifts over to the series resistance and causes a peak in the signal current. The maximum potential drop over the pn junction is 16 mV.

Figure 5a shows internal hot carrier populations and external signal current at the lowest intensity level, with the external resistance now raised to 500 Ω . No oscillations are visible, and the laser pulse shape is readily identifiable. In Fig. 5b, we observe that an increased laser intensity by an order of magnitude again results in strong oscillations which continue for a long while after the laser pulse has ended. The oscillation period increases to 250 ps, also with some timing jitter. Saturation and the increased series resistance reduce the electric field, extending the junction transit time. The potential drop over the pn junction amounts to 7 mV

towards the end of the laser pulse, but peaks of 35 mV can be observed during the pulse.

Figure 6a shows the hot carrier population inside the pn junction and the signal current from the APD, with an external resistance of 3 k Ω at the lowest irradiation level.

In Fig. 6b, we observe that an increased laser intensity by an order of magnitude does not induce oscillations in the signal current. After an initial overshoot in the hot carrier populations, the increased series resistance stabilizes the signal current by restricting and thermalizing the hot carriers at both ends of the depletion zone. Accumulated, thermalized carrier populations at both ends of the depletion zone produce a steady, strong signal, although this accumulation weakens subsequent carrier production, as can be seen from the falling hot hole curve in Fig. 6b. The potential drop over the pn junction towards the end of the laser pulse was 32 mV.

Figure 7a shows hot carrier populations inside the pn junction and signal current from an APD with external resistance of 32 k Ω at the lowest irradiation level.

Figure 7b demonstrates that an augmented laser intensity by an order of magnitude does not result in ripples in the signal current. However, the initial overshoot in the carrier populations is still present. After the overshoot, the hot electron population falls rapidly, and temporarily even drops below that of the lower intensity case during parts of the laser pulse. In this case, the average potential drop over the pn junction amounts to 80 mV towards the end of the laser pulse.

For the highest irradiation level and the highest external resistances of 3 k Ω and 32 k Ω , the conditions for new carrier generation become poor after an initial overshoot, and we can see some after-pulsing in the drifting hot electron population inside the depletion zone, especially for the 32-k Ω case. Because the high-intensity 73,000 photons/ns simulations were carried out using superparticles (one superparticle equals 10 real electrons or holes), our particle resolution of 10 electrons (holes) became somewhat coarse for that particular case. We see from Fig. 7b that the hot drifting junction electrons repeatedly reach numbers as low as 10 or less, i.e., we are operating at our lower particle resolution limit. The high resistances severely disturb the production of new avalanche electrons, so impact ionization may temporarily halt due to lack of active electrons in the multiplication zone. However, simultaneously, partly due to the high input levels and partly due to device design, some accumulated photogenerated electrons in distant parts of the absorption layer may revive impact ionization again. This will affect all the cases studied here. Although the production of avalanche carriers may suddenly stop, and then resume again, these disturbances are not severe enough to show up as after-pulsing in the signal current of Fig. 7, because the APD is already saturated with long since thermalized avalanche-generated

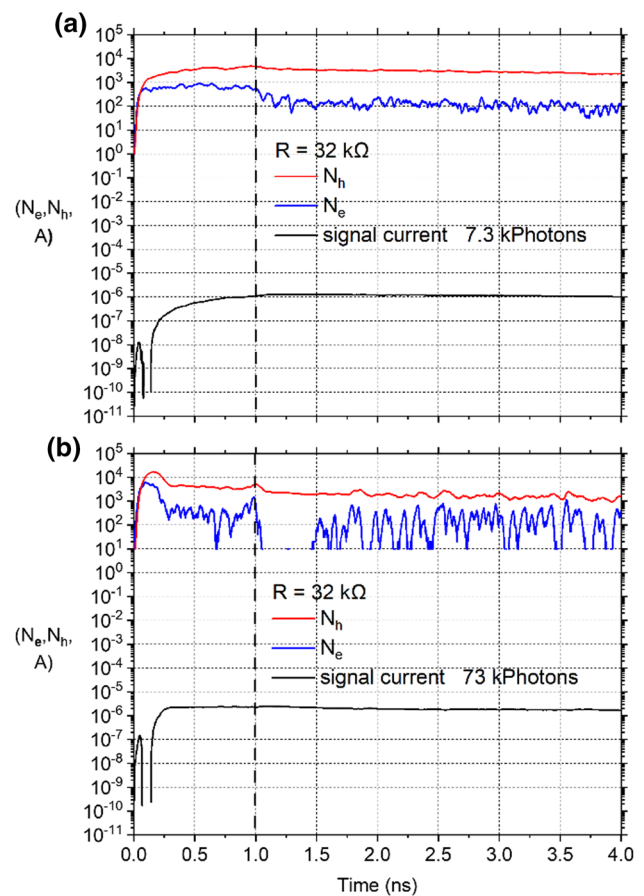


Fig. 7 Signal current (in amps) (bottom curve) and hot carrier populations (upper curve N_h holes, middle curve N_e electrons) under way inside the pn depletion zone for an avalanche photodiode with external resistance of 32 k Ω at (a) the lowest irradiation level of 7.3 kPhotons in 1 ns. (b) Increased laser intensity by an order of magnitude exposes mild afterpulsing in the electron population; however, not visibly affecting the signal current. In both parts of the figure, the dashed vertical line indicates the end of the laser pulse.

carriers leaving the depletion zone, thus keeping the external current flowing evenly.

As indicated in the earlier sections, the oscillatory effects demonstrated here cannot be fully reproduced by “static” bias voltage/avalanche gain curves which only show the gain as a function of a static junction voltage bias. In those curves, the junction voltage is due to a “global” pn junction field which is imposed by an external voltage source, and the curves are obtained by integrating over time. Rather, the modulation of the gain just demonstrated also includes the important local and dynamic effects: a reduction of the electric field nucleates in the region between the generated charges and temporarily pinches off avalanche gain in a critical location. For the two lowest values of the series resistance, this begins near the upper part of the multiplication zone where the bias electric field is lower. The local electric field oscillates with the same period of 220–250 ps as

observed earlier, with a maximum reduction of 0.23–0.24 kV/cm between the separating electron and hole ensembles. Depending on the position, this means that 3–100% of the bias electric field strength periodically vanishes here. The “global” junction voltage is less affected by this field perturbation, showing only a peak value of 16 mV for the intrinsic case and 35 mV for the 500 Ω case. For the highest series resistance, the local electric field reduction reaches quite similar values, but, interestingly, the domain for the reduction is now rather stable, covering most of the multiplication zone with no oscillations, just varying very slowly in time, and there is also a more sizeable “global” junction voltage reduction of 80 mV.

These few examples should be representative for the onset of nonlinear gain response of an APD with different resistive elements in the external circuit while exposed to high-level radiation from a laser pulse with finite duration. There can be other capacitive and even inductive elements in the external readout circuits which could equally well affect the APD signal, and they could also have been simulated. These passive circuit elements are connected to the geometrical configuration of the APD surroundings, the length of wires, wire bonding versus indium bump mounting, and so on. Active elements, transimpedance amplifier issues causing ringing behavior, belong to another category of problems. To keep matters simple, we have restricted ourselves to a single type of external impedance. Mapping out APD responses for many types of readout circuits is a somewhat larger task.

Conclusions

We have investigated the nonlinear signal current response for a HgCdTe APD with external resistances irradiated by finite-duration laser pulses. It has been shown that high-intensity irradiation delivered in the form of a 1-ns laser pulse could readily induce correlated current and hot carrier number oscillations under certain conditions. Being caused by hot carriers underway in the pn junction, these oscillations are related to the transit time, i.e., for the present case, they should occur for external series resistances lower than 3 k Ω . Above this value, a transition occurs as resistances increase further, where the oscillations are damped out due to strong restriction of the external signal current and the accumulation of thermalized carriers at both ends of the pn junction.

There is a feedback mechanism where the avalanche gain creates two separating hot charge ensembles which screen out a small portion of the junction bias, causing part of the junction voltage to shift over to the series resistance, which increases the external signal current but temporarily reduces the avalanche gain. The reduced gain eventually causes the voltage shift to return onto the junction, increasing the

momentary avalanche gain but reducing the external signal current. As the next perturbation in avalanche-generated charges develops and the charges separate, part of the bias voltage shifts over to the external resistance again, increasing the external signal current again, and so on. A finite series resistance is needed for defining this net voltage drop over the pn junction.

Depending on the value of the external series resistance and the irradiation level, we have demonstrated how oscillations or periodic ripples in the signal current gradually develop, not only during the laser pulse itself but also how they continue to evolve for a short period after the laser pulse has ended, while the APD is still saturated by ongoing generation of new internal charge carriers.

Conflict of interest The authors declare that they have no conflicts of interest.

Open Access This article is licensed under a Creative Commons Attribution 4.0 International License, which permits use, sharing, adaptation, distribution and reproduction in any medium or format, as long as you give appropriate credit to the original author(s) and the source, provide a link to the Creative Commons licence, and indicate if changes were made. The images or other third party material in this article are included in the article's Creative Commons licence, unless indicated otherwise in a credit line to the material. If material is not included in the article's Creative Commons licence and your intended use is not permitted by statutory regulation or exceeds the permitted use, you will need to obtain permission directly from the copyright holder. To view a copy of this licence, visit <http://creativecommons.org/licenses/by/4.0/>.

References

1. G. Perrais, S. Derelle, L. Mollard, J.-P. Chamonal, G. Destefanis, G. Vincent, S. Bernhardt, and J. Rothman, Study of Transit-Time Limitations of the Impulse Response in Mid-wave Infrared HgCdTe Avalanche Photodiodes. *J. Electron. Mater.* 38, 1790 (2009).
2. A. Singh and R. Pal, Impulse Response Measurement in the HgCdTe Avalanche Photodiode. *Solid State Electron.* 142, 41 (2018).
3. J. Rothman, K. Foubert, G. Lasfargues, and C. Largeton, Response Time Measurements in Short-wave Infrared HgCdTe e-APDs. *J. Electron. Mater.* 43, 2947 (2014).
4. M.D. Eisaman, J. Fan, A. Migdall, and S.V. Polyakov, Single-Photon Sources and Detectors. *Rev. Sci. Instr.* 82, 071101 (2011).
5. X. Jiang, M. Itzler, K. O'Donnell, M. Entwistle, M. Owens, K. Slomkowski, and S. Rangwala, InP-Based Single-photon Detectors and Geiger-mode APD Arrays for Quantum Communications Applications. *IEEE J. Selected Topics in Quant. Electron.* 21, 3800112 (2015).
6. J. Asbrock, S. Bailey, D. Baley, J. Boisvert, G. Chapman, G. Crawford, T. de Lyon, B. Drafahl, J. Edwards, E. Herrin, C. Hoyt, M. Jack, R. Kvaas, K. Liu, W. McKeag, R. Rajavel, V. Randall, S. Rengarajan, and J. Riker, Ultra-High Sensitivity APD based 3D LADAR Sensors: Linear Mode Photon Counting LADAR Camera for the Ultra-Sensitive Detector Program. *Proc. SPIE* 6940, 69402O (2008).

7. M. Jack, G. Chapman, J. Edwards, W. Mc Keag, T. Veeder, J. Wehner, T. Roberts, T. Robinson, J. Neisz, C. Andressen, R. Rinker, D.N.B. Hall, F. Amzajerdian, and T.D. Cook, Advances in LADAR Components and Subsystems at Raytheon. *Proc. SPIE* 8353, 83532F (2012).
8. S. Pes, J. Rothman, P. Bleuet, J. Abergel, S. Gout, P. Ballet, J.-L. Santailier, J.-A. Nicolas, J.-P. Rostaing, S. Renet, A. Vandeneuynde, L. Mathieu, and J. Le Perchec, Reaching GHz Single Photon Detection Rates with HgCdTe Avalanche Photodiodes Detectors. *Proc. SPIE* 11852, 118525S (2021).
9. S.M. Sze, and M.-K. Lee, *Semiconductor Devices: Physics and Technology*, 3rd ed., (Hoboken: Wiley, 2012).
10. A.K. Storebø, and T. Brudevoll, Modeling of a Back-Illuminated HgCdTe MWIR Avalanche Photodiode with Alloy Gradients. *J. Phys: Conf. Ser.* 647, 012051 (2015).
11. M. Moresco, F. Bertazzi, and E. Bellotti, GaN Avalanche Photodetectors: A Full Band Monte Carlo Study of Gain, Noise, and Bandwidth. *IEEE J. Quant. Electron.* 47, 447 (2011).
12. A.K. Storebø, D. Goldar, and T. Brudevoll, Simulation of Infrared Avalanche Photodiodes from First Principles. *Proc. SPIE* 10177, 101771B (2017).
13. B. Li, H. Ye, J. Chu, and S. Krishnamurthy, Logarithmic Approximation for the Energy Band in Nonparabolic Semiconductors. *J. Appl. Phys.* 83, 7668–7671 (1998).
14. Program ABINIT, <http://www.abinit.org/>
15. B.K. Ridley, *Quantum Processes in Semiconductors* (Oxford, 1999).
16. M.M. Hayat, W.L. Sargeant, and B.E.A. Saleh, Effect of Dead Space on Gain and Noise in Si and GaAs Avalanche Photodiodes. *IEEE J. Quant. Electron.* 28, 5 (1992).
17. D.C. Herbert, P.A. Childs, R.A. Abram, G.C. Crow, and M. Walmsley, Self-Consistent 2-D Monte Carlo Simulations of InSb APD. *IEEE Trans. Electr. Dev.* 52, 2175 (2005).

Publisher's Note Springer Nature remains neutral with regard to jurisdictional claims in published maps and institutional affiliations.